Design of a Dual Wide-Angle Visual Cue Simulator

J. L. COPELAND,* W. M. KAHLBAUM JR.,† L. E. BARKER JR.,‡ G. G. STEINMETZ,‡ AND R. D. GROVE‡
NASA Langley Research Center, Hampton, Va.

The simulator design provides independent, simultaneous visual environment and pilot flight stations, allowing research to be conducted with two piloted vehicles in a differential mode, either cooperative or noncooperative. Attention is given to design features including: the pilot's field of view, occlusion and parallax in the observed scene, and maximum range of simulated flight parameters. In parallel to a detailed design phase, extensive analyses and computer simulations have been conducted using actual design parameters. These studies were directed toward: 1) development of the drive equation for an offset four-axis gimbal system, 2) evaluation of the effects of torque coupling between axes of four-gimbal systems, and 3) the achievement of scene synchronization through matching the dynamic responses of independent servomechanisms.

Nomenclature

$I_{x\alpha}$ = moment of inertia of fourth-axis gimbal about its x axis (of rotation), ft-lb-sec^2
$I_{x\theta}$ = moment of inertia of pitch gimbal about its x axis, ft-lb-sec^2
$I_{y\theta}$ = moment of inertia of pitch gimbal about its y axis (of rotation), ft-lb-sec^2
$I_{z\theta}$ = moment of inertia of pitch gimbal about its z axis, ft-lb-sec^2
$I_{x\phi}$ = moment of inertia of roll gimbal about its x axis (of rotation), ft-lb-sec^2
$I_{y\phi}$ = moment of inertia of roll gimbal about its y axis, ft-lb-sec^2
$I_{z\phi}$ = moment of inertia of roll gimbal about its z axis, ft-lb-sec^2
$I_{x\psi}$ = moment of inertia of yaw gimbal about its x axis, ft-lb-sec^2
$I_{y\psi}$ = moment of inertia of yaw gimbal about its y axis, ft-lb-sec^2
$I_{z\psi}$ = moment of inertia of yaw gimbal about its z axis (of rotation), ft-lb-sec^2
$L_{\theta\phi}$ = coupled torque applied to the pitch gimbal about its x axis from the roll gimbal, ft-lb
$L_{\psi\theta}$ = coupled torque applied to the yaw gimbal about its x axis from the pitch gimbal, ft-lb
$M_{\phi\alpha}$ = coupled torque applied to the roll gimbal about its y axis from the fourth-axis gimbal, ft-lb
$M_{\psi\theta}$ = coupled torque applied to the yaw gimbal about its y axis from the pitch gimbal, ft-lb
$N_{\theta\phi}$ = coupled torque applied to the pitch gimbal about its z axis from the roll gimbal, ft-lb
$N_{\phi\alpha}$ = coupled torque applied to the roll gimbal about its z axis from the fourth-axis gimbal, ft-lb
$P_\theta,Q_\theta,R_\theta$ = instantaneous angular rates of pitch gimbal about its x, y, and z body axes, respectively, rad/sec
$\dot{P}_\theta,\dot{Q}_\theta,\dot{R}_\theta$ = instantaneous angular accelerations of pitch gimbal about its x, y, and z body axes, respectively, rad/sec^2
P_ϕ,Q_ϕ,R_ϕ = instantaneous angular rates of roll gimbal about its x, y, and z body axes, respectively, rad/sec
$\dot{P}_\phi,\dot{Q}_\phi,\dot{R}_\phi$ = instantaneous angular accelerations of roll gimbal about its x, y, and z body axes, respectively, rad/sec^2
P_ψ,Q_ψ,R_ψ = instantaneous angular rates of yaw gimbal (transparency) about its x, y, and z body axes, respectively, rad/sec
$\dot{P}_\psi,\dot{Q}_\psi,\dot{R}_\psi$ = instantaneous angular accelerations of yaw gimbal (transparency) about its x, y, and z body axes, respectively, rad/sec^2
T_α = fourth-axis gimbal drive torque, ft-lb
T_θ = pitch gimbal drive torque, ft-lb
T_ϕ = roll gimbal drive torque, ft-lb
T_ψ = yaw gimbal drive torque, ft-lb
α = fourth-axis gimbal angle, rad
$\dot{\alpha}$ = fourth-axis gimbal angular rate, rad/sec
$\ddot{\alpha}$ = fourth-axis gimbal angular acceleration, rad/sec^2
β = fourth-axis gimbal offset angle, rad
$\Delta x,\Delta y,\Delta z$ = angular separations between target and horizon images in the x, y, and z directions, deg
θ = pitch gimbal angle, rad
$\dot{\theta}$ = pitch gimbal angular rate, rad/sec
$\ddot{\theta}$ = pitch gimbal angular acceleration, rad/sec^2
ϕ = roll gimbal angle, rad
$\dot{\phi}$ = roll gimbal angular rate, rad/sec
$\ddot{\phi}$ = roll gimbal angular acceleration, rad/sec^2
ψ = yaw gimbal angle, rad
$\dot{\psi}$ = yaw gimbal angular rate, rad/sec
$\ddot{\psi}$ = yaw gimbal angular acceleration, rad/sec^2

1. Introduction

IN late 1966 the NASA Langley Research Center embarked on a program to develop a dual cockpit, fixed-base simulator with a wide-angle visual display allowing the two simulated vehicles to operate separately or in a differential mode. One of the basic criteria in the display design was that each vehicle's image be free to move over the entire field of view while still maintaining correct positioning of the inertial horizon (sky-Earth) reference and correct aspect of the target image. In an effort to overcome the classic gimbal lock problem in the visual display, a four-axis gimbal system is employed in both the sky-Earth projection system and the target image generation system. To reduce optical shadowing and occlusions caused by the gimbals to a minimum, the fourth axis is offset at 30° rather than 90° as is common in a four-gimbal system. Although the offset four-gimbal configuration is not unique, the mathematical model for driving the gimbal is a new development.

No effort has been made to eliminate singularities from the two-axis target image (mirror) projection system. The point of discontinuity in the mirror system has been removed from the pilot's normal field of view by tilting the entire projection system. Target ranging is simulated by the use of simul-

Presented as Paper 70-360 at the AIAA Visual and Motion Simulation Technology Conference, Cape Canaveral, Fla., March 16–18, 1970; submitted April 24, 1970; revision received October 16, 1970.

* Aero-Space Technologist, Simulator Development Section, Analog Computing and Simulation Branch, Analysis and Computation Division. Member AIAA.

† Aero-Space Technologist, Simulator Development, Analog Computing and Simulation Branch, Analysis and Computation Division.

‡ Aero-Space Technologist, Analog Computing Section, Analog Computing and Simulation Branch, Analysis and Computation Division.

taneously driven zoom lenses in both the target image generation and target projection systems.

Improved dynamic synchronization between the sky-Earth and target images is being sought by matching all servos to the same dynamic response characteristics.

This paper will describe the simulator systems, present highlights of the over-all design effort and cover details of studies carried out at Langley in developing the sky-Earth four-gimbal system.

2. System Description

2.1 Basic System

The simulator is designed for installation and operation in the Flight Control Research Facility at NASA's Langley Research Center. In addition to varied simulator hardware, this facility houses all of Langley's scientific computing equipment. The basic hardware of this simulator will consist of the cockpits and scene projectors which will reside in two 40-ft-diam projection spheres as shown in Fig. 1. All computir g will be performed on a CDC 6600 computer operating in real time with its existing analog-to-digital interface. A control console located between the two spheres will provide the necessary interface of the two systems (A and B) with the computer as well as providing the operator's monitor and control station. The target image will be presented in black and white, and the sky and earth will be blue and mottled brown, respectively, with a white haze band at the horizon. The pilot's field of view is 340° in the horizontal and extends vertically from directly overhead to 60° below the horizon.

Each simulator system consists of three major subsystems: the cockpit, target subsystem, and sky-Earth-sun subsystem.

2.2 Cockpit

A basic single place cockpit (Fig. 2) was designed with maximum versatility to allow for quick canopy and instrumentation changes. The design is a welded tubular frame furnished with a basic instrument panel, a programable three-axis control loading system, and basic secondary controls. Each cockpit is equipped with a pressure feedback servo to allow control of a standard pressure (g) suit. The cockpit structure is mounted on a buffet mechanism that moves the pilot's eye point on a virtual radius arm fixed at the projection screen surface to avoid parallax errors. The buffet system is capable of producing accelerations up to ± 1 g at frequencies up to 20 Hz.

2.3 Target Subsystem

The target subsystem consists of two main sections, the target image generator and the target projector, as illustrated in Fig. 3. This subsystem presents each pilot with the image of the other, correctly positioned in line of sight and aspect, and correctly sized (visual angle) over a relative simulated range of 300–45,000 ft. The target image generator consists of a standard black and white 1029 line TV vidicon camera viewing a 120–1 scaled model through a commercial zoom lens limited to a 15–1 useful zoom range. There is no physical motion of the camera, so the perspective of the target image is correct at only one range; the range selected is 800 ft. The target model is mounted in an offset, four-axis gimbal system that allows all-attitude positioning of the model. The TV camera is positioned to avoid occlusion of the target model by the gimbal hubs. The model is illuminated by four, 250-w, quartz-iodide lamps which are positioned to eliminate shadowing of the model.

The target image projector consists of a high-brightness, high-resolution cathode ray tube, a large format zoom lens with a 10–1 magnification range and a mirror drive system employing separate azimuth and elevation drives. The cathode ray tube is capable of a highlight brightness of 10,000 ft Lamberts. The zoom lens has an 8.5-in.-diam exit pupil and is designed with a minimum resolution at least twice that of the human eye throughout the zoom range. This resolution limit is referred to the screen, as seen by the observer at the center of the sphere. Since the location of the lens in the sphere creates a varying throw distance, a focus servo is required (in addition to the zoom servo) to maintain focus of the projected image. The lens elements are coated with high-efficiency, low-reflecting coatings resulting in a total transmission efficiency of 70%. The resulting target brightness at minimum range (300 ft) is 0.5 ft Lambert increasing to 1.0 ft Lambert at maximum range. The two-axis mirror system allows continuous positioning of the target within the limits of the field of view. The entire target projection system is mounted at a 25° inclination to the sphere horizontal to place the discontinuity of the mirror gimbals outside the normal

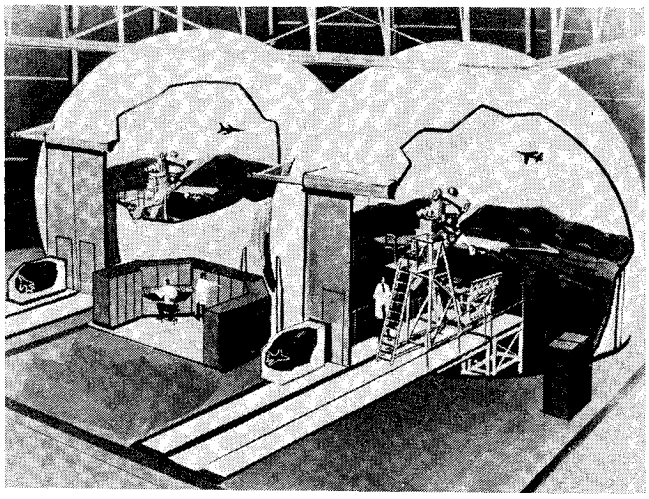

Fig. 1 Dual wide-angle visual cue simulator.

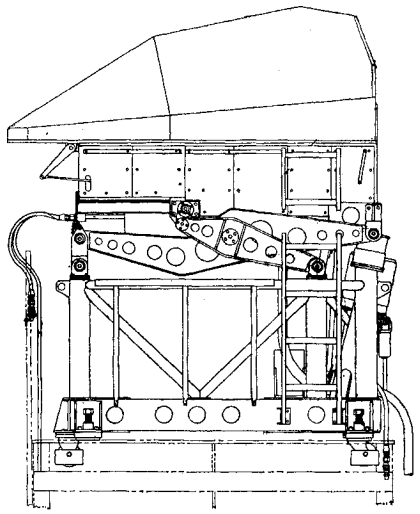

Fig. 2 Cockpit general arrangement.

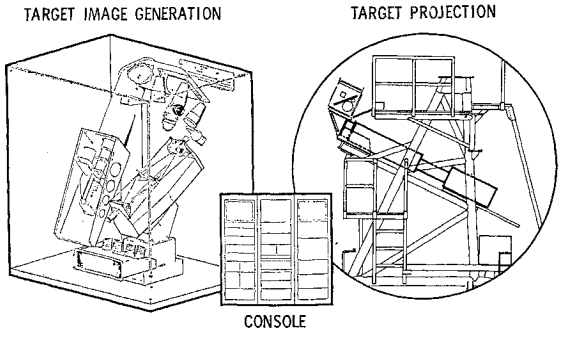

Fig. 3 Target image generator and projector.

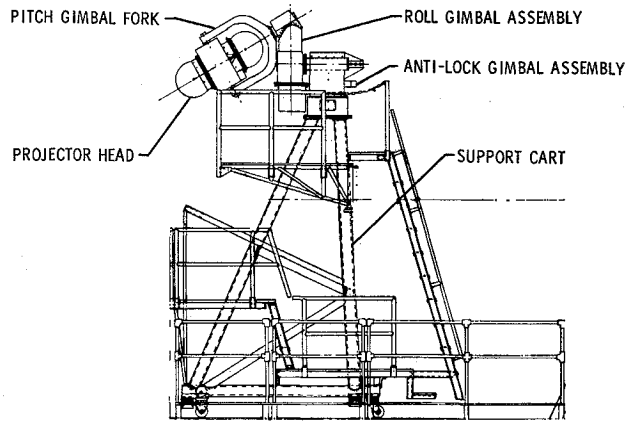

Fig. 4 Sky-Earth-sun projector general arrangement.

field of view. All servo drives in the target subsystem employ d.c. torque motors closely coupled to the load and have precision d.c. potentiometer and d.c. tachometer feedbacks. The mirror drives employ combined position and rate commands.

2.4 Sky-Earth-Sun Subsystem

The inertial reference cue for each vehicle is provided by a sky-Earth-sun projector mounted in an offset, four-axis gimbal system, which in turn is mounted on a rigid, tubular, A-frame structure (see Fig. 4). The projector head is illustrated in more detail in Fig. 5, which shows the 18-in.-diam hemispherical transparencies mounted on the innermost gimbal and illuminated by separate point light (mercury vapor) sources. This system provides a direct optical projection of the sky and terrain over the entire field of view. The projected highlight brightness is nominally 0.04 ft Lambert for proper contrast with the target. Because of the offset location of the projector with respect to the sphere center and the separation of the transparency spheres, the light sources are mounted on a three-axis rectilinear servo drive to provide correct mapping on the projection screen. A sun projector is provided which positions the sun at the zenith position. The sun disk is optically projected to form a spot of light subtending approximately $\frac{1}{2}^\circ$ with sufficient brightness to wash out the target but not bright enough to cause visual impairment. The sun drive is connected to the rectilinear light drives by a linkage that provides a mechanical analog of the vector between the light source and transparency zenith. The two outer gimbals utilize rotary hydraulic drives and the two inner gimbals and the three rectilinear servos utilize electric torque motor drives. These drives, like the target subsystem drives, use precision d.c. feedbacks. The gimbal position commands are augmented by rate command inputs.

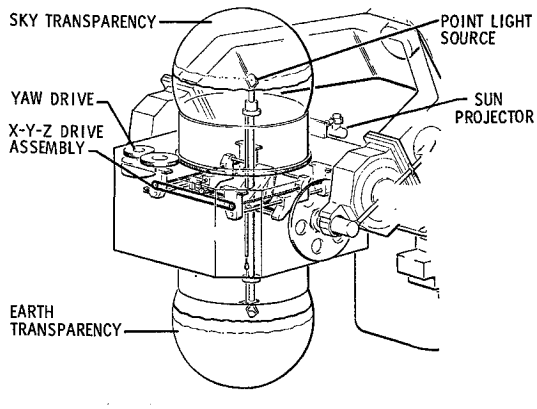

Fig. 5 Sky-Earth-sun projector head.

2.5 Control Console

The control console houses all controls and electronics for the entire system. In addition to the normal functions, the control console provides complete system test capability and full-time metering of all servo positions and tracking errors to allow rapid assessment of system status.

3. Computing Considerations

The computer program is being deveioped as a modular approach whereby each mathematical subsystem, such as rigid body equations of motion, aerodynamics, engines, SAS, and so forth, is essentially a subroutine that can be called by the main computer program and assembled as a specific aircraft. The aerodynamic coefficients have been written in a general form such that changing from one vehicle to another only requires new data. In the math model of the relative geometry (see Fig. 6), a line-of-sight axis system is developed relative to the second vehicle in terms of rotations dictated by the first aircraft position. The attitude of aircraft A (and B) relative to the inertial reference is determined by integration of differential equations involving its rotational rates. Quaternions are used in describing the orientation to allow all possible attitudes to be computed.[1] The resulting transformation matrices are presented to the interface computing as direction cosines.

4. Interface Computing

In addition to the equations of motion and relative geometry of the two vehicles, the computer program includes the computations required by the several hardware subsystems. This interface computing can be broken down into three areas determined by the simulator hardware subsystems. These include the sky-Earth-sun, the target, and cockpit subsystems.

4.1 Sky-Earth-Sun Subsystem Computations

Computations are included to convert the direction cosines of the vehicle body axis system (relative to the inertial reference frame) into specific gimbal angles for the offset, four-axis system. This is accomplished by equating the direction cosines to the equivalent transformation in terms of the hardware gimbal angles. Determination of the fourth-axis gimbal position command is a prerequisite to these computations and will be discussed at greater length later in the paper. The three rectilinear lamp drives can be determined geometrically once the gimbal angles are known. Because of the rate augmented servos of the SES system, auxiliary equations are included to provide rotational rate commands to each of the gimbals.

4.2 Target Projector Subsystem Computations

Computations are included which convert the direction cosines relating the aircraft body axis systems to each other and to the inertial system into specific mirror and target model

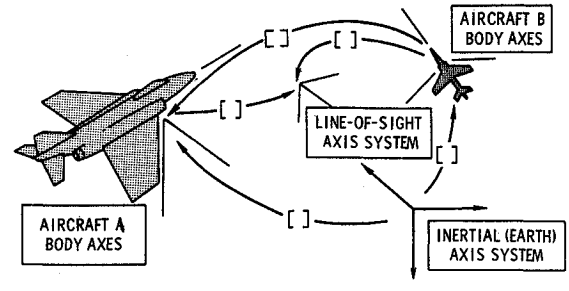

Fig. 6 Definition of axis systems.

gimbal angles. Computations are also included which relate 1) the camera and projector lens zoom functions to target range and 2) projection lens focus drive to the image projector throw distance. Among the parameters considered are 1) the derotation of the apparent roll of the target model due to mirror rotations, 2) variations of zoom position (magnification) as a function of varying projection distance (due to mirror motion), and 3) the constant tilt angle of the entire target projection system.

4.3 Cockpit Drives

Computations are carried out for all of the flight instruments including the three gimbal axes of the attitude indicator. Buffet severity is determined in order to modulate the buffet servo and normal acceleration is used to drive the "g" suit servo.

5. Concept Formulation

In establishing the system concept and performance specifications, a major consideration was that the hardware should be firmly within limits of the state-of-the-art existing at that time. To accomplish this, a parallel approach was taken. First, an in-house team conducted both breadboard evaluations and subjective testing to establish limits of performance requirements and evaluation of specific design approaches. Second, a study contract was carried out by the Northrop Aircraft Division (formerly Norair Division) to provide additional design analysis. As a first step, a set of vehicle performance data was compiled by the LRC team, which considered not only the minimum and maximum requirements of past work but, in addition, took into consideration the requirements of future vehicles to the extent possible. The maximum vehicle rates and accelerations shown in Table 1 appeared to satisfy these requirements.

Static subjective tests were carried out initially to establish the minimum visual factors for the specification. These tests established parameters such as minimum contrast between target and background, minimum acceptable absolute brightness levels, and minimum acceptable resolution of the target. Obviously, lower background levels allow lower target brightness levels, as may be seen in Fig. 7. This figure also shows where the light levels of the final projection system fall. Subjective tests, run in a prototype simulator at Langley, concluded that these levels are quite acceptable under dynamic flight conditions, although the static tests had argued for higher levels.

The final design concept was formulated after examining a number of possible tradeoffs. Several approaches for translating the Earth scene were considered but rejected because of the development nature of the design. The present design of separate sky and Earth projectors will allow later addition of the moving terrain. Cockpit motion other than buffet was rejected because of complexity. Provisions have been made in the cockpit design to allow future addition of limited motion. Virtual image viewing was rejected on the basis that the existing 40-ft-diam spheres would provide adequate eye relief over a wide field of view. Direct optical projection of the target image from a scaled model was seriously considered but discarded because of depth of field and low light-level problems. Direct television projection from a high-intensity cathode ray tube was then chosen on the basis of satisfactory performance in other simulators. The Dalto-RCA 6-in.-diam CRT used in current Amphicon projectors was selected as providing the highest combination of brightness and resolution available at the time. Mechanization of target ranging by simultaneous drive of the camera and projection zoom lenses was chosen over raster shrinkage or camera range bed motion as being the most feasible for the range excursions to be simulated. Simultaneous motion of the two lenses was selected to avoid switchover at mid range.

Table 1 Maximum vehicle performance

Quantity	Maximum value
Roll rate, p	8.0 rad/sec
Roll acceleration, $\dot{p}$	10.0 rad/sec^2
Pitch rate, q	3.0 rad/sec
Pitch acceleration, $\dot{q}$	3.0 rad/sec^2
Yaw rate, r	3.0 rad/sec
Yaw acceleration, $\dot{r}$	3.0 rad/sec^2
Range	300–45000 ft
Range rate	6000 fps
Normal acceleration	$+10$ to $-3g$
Lateral acceleration	$\pm 3g$
Relative rate of climb	3000 fps
Individual rate of climb	2000 fps

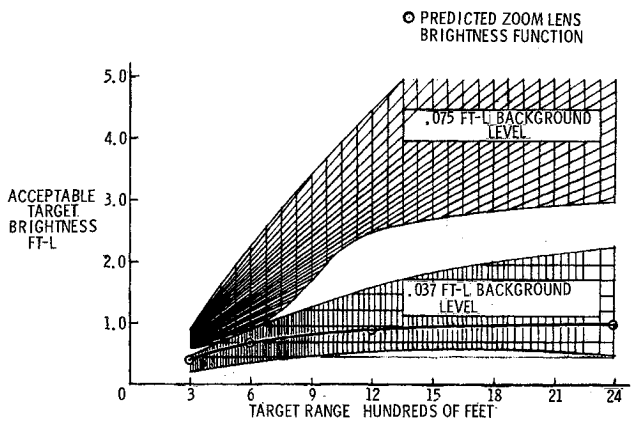

Fig. 7 Target brightness subjective static tests.

6. Design Analyses

In the detailed design analysis, as in the concept formulation phase, parallel efforts were carried out by the contractor team and the LRC team. The contractor effort was mainly devoted to developing the design of the various servo systems. Details concerning weights, inertias, friction, gearing errors, and structural analyses were considered in the final over-all design. The parallel effort carried out by the LRC team used the results of the detailed servo design to carry out an extensive simulation program. First, the basic servos were simulated on a single-axis basis to verify the design. Then a complete simulation of the four-axis gimbal system was performed, which will be described in more detail in the second half of this paper. Another computer study was carried out to determine locations of the two projectors that would result in minimum occlusions of the projected images. As an aid in the final design of the projection zoom lens, two separate studies were carried out at Langley. The first was an accurate survey of the faceplate curvatures of three cathode ray tubes from a typical manufacturing run. The second was a measurement of the spectral output of these tubes.

7. Four-Axis Gimbal and Scene Synchronization Studies

To avoid generating false visual cues, the simulator was designed to minimize all sources of parallax errors between the target image and the sky-Earth scene. In a static situation, this can be accomplished by proper attention to projector geometry. However, it is also necessary to maintain minimum parallax errors over a wide dynamic range. The basic approach to this dynamic synchronization problem has been to match all servos to the same second-order response, one which has nearly linear phase shift (i.e., constant time delay over the frequency spectrum of interest). Another source of

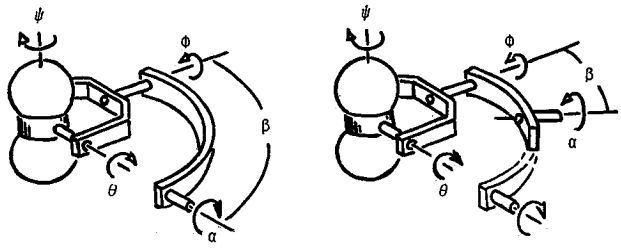

Fig. 8 Gimbal system definitions.

synchronization error in a three-axis gimbal system is the magnitude of rates and accelerations encountered as gimbal lock is approached. These can easily reach slew rate and stall force limits. Short of these limits, torque coupling between axes can cause load disturbances that result in visible transients in even the stiffest servo designs.

To avoid the gimbal lock problem, a four-axis system is being employed. Since the four-axis system entails a degree of redundancy, the problem arises of how best to formulate the fourth-axis command. Use of this type of system does not eliminate concern over the effects of torque coupling between axes under dynamic conditions. In an effort to solve these problems, a complete simulation of the sky-Earth four-axis system and target mirror system has been carried out. This simulation has also been used to verify the maximum rate and acceleration capabilities of the sky-Earth system design. No studies of the target model four-axis system have been undertaken since its response is not pertinent to the synchronization problem.

8. Four-Axis Gimbal Studies

The first portion of the study has concerned with the formulation of the fourth-gimbal drive command. Figure 8 illustrates two forms of the four-gimbal system. Since the inner three gimbals constitute a three-axis system, in either case the motion of the fourth gimbal should maintain the middle (θ) gimbal angle at a minimum value to minimize the high gimbal rates which occur if gimbal lock is approached. In the case of $\beta = 90°$, it is theoretically possible to maintain $\theta = 0$ for any attitude of the transparencies. Also, in this case the maximum gimbal rates are limited to the value of the total rotation rate vector. In the offset four-axis gimbal system with $\beta < 90°$, neither of these statements is true. Now there exist orientations of the transparencies for which no position of the α gimbal can reduce the θ gimbal angle to zero. Also, the maximum gimbal rates approach those of a three-axis system as β approaches zero. The reason for choosing the offset system for the visual display is that it reduces the optical shadow that can be cast by the hub of the pitch gimbal. Clearly, then, the introduction of any value of β other than 90° is a tradeoff between gimbal rates and optical shadows. In this system the choice of $\beta = 30°$ was made on the basis of minimizing the optical shadows. The studies carried out were then able to determine the maximum rates which would be encountered.

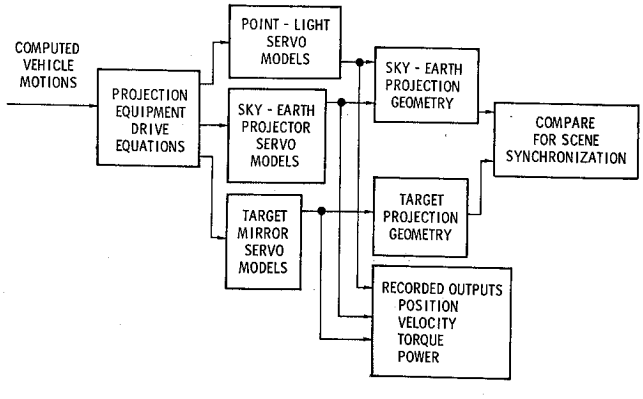

Fig. 9 Simulation of projection equipment subsystem.

8.1 Fourth Gimbal Drive Model

In the development of the offset fourth-axis drive, the transformation between the nonrotating axis system and the axis system rotating with the transparencies may be expressed in terms of the gimbal angles.

$$[C] = [\psi]_z[\theta]_y[\phi]_x[\beta]_y[\alpha]_x$$

This equation may be written as:

$$[\psi]_z[\theta]_y[\phi]_x = [C][\alpha]_x^{-1}[\beta]_y^{-1} \tag{1}$$

The direction cosine matrix $[C]$ in Eq. (1) is the input from the central computer program. Since β is a known constant, the only unknown on the right side of Eq. (1) is α. Once α is determined, the remaining three gimbal angles can be determined algebraically using standard Euler angle resolving methods.

The basic problem, then, is to determine the outer gimbal angle in some prescribed manner. Here the basic method developed by Wilson[2,3] may be applied to develop the proper drive equation as:

$$\begin{aligned} \dot{\alpha} &= f(\theta)\ \mathrm{sgn}(-\sin\theta \sin\phi) \\ f(\theta) &= K|\sin\theta| \end{aligned} \tag{2}$$

The basic magnitude function $f(\theta)$ was empirically determined. On the surface, the reasoning used for the four-axis system appears quite valid and adequate for the offset model. However, an undesirable effect is noted under static conditions. Unlike the four-axis system for which the reasoning was derived, the 30° offset system has situations for which the minimum of the middle gimbal angle θ is not zero but some value between zero and 60°. Then clearly there are situations in which the middle gimbal is at its minimum angular position and the magnitude of the drive equation is nonzero, due to the ($\sin\theta$) term. Since the passage through the proper position of the fourth axis resulting in minimum θ is accompanied by a sign change in the drive equation (because of the $\sin\phi$ term in the sgn function), the resulting action of the drive equation is an oscillation (limit cycle) about the actual minimum with the amplitude depending upon the gain being employed and the value of the actual minimum angle of the middle gimbal.

Several approaches to correct or modify this undesirable motion are available. The first approach is to recognize the region where the sine cannot be minimized to zero and then impose a constraint on $\dot{\alpha}$ which sets it to zero whenever the function $K(\sin\theta)$ cannot be driven to zero. This method, in effect, allows one to minimize θ to two different levels, one at 0° and the other at 60°. Although this method worked satisfactorily in many cases, in certain gimbal orientations an interaction developed between the constraint and the basic equation, which led to violet transient motions.

A second approach, which does not appear to be subject to these transients, is to constrain the θ gimbal to motion within a 60° cone. Thus, the drive equation is tailored for only one level and may be expressed as

$$f(\theta) = K[H(60° - \theta)] \tag{3}$$

where

$$H = 0 \text{ if } |\theta| < 60°$$
$$H = 1 \text{ if } |\theta| \geq 60°$$

This approach has shown no ill effects, such as the instabilities experienced by the first, and still eliminates the limit cycle motion encountered in the original formulation. The problem associated with this approach is how to filter the onset of the fourth gimbal motion, such that the velocities, accelerations, and torque coupling induced in the system by the fourth-axis motion are kept reasonably low and smooth. Several systems of first-order filters were used in an effort to solve this problem but the resulting degree of improvement was small. Further experimentation has led to the following form of gimbal drive:

$$f(\theta) = [H(60° - \theta)][K \sin(|\theta| - 60°)] \quad (4)$$

This form provides a very definite improvement over any of the other forms, and a comparison between Eqs. (3) and (4) will be made in the section of this paper dealing with test cases.

8.2 Gimbal Simulation

In parallel with the development of the gimbal drive model, a simulation of the gimbal servos and projection geometry was developed. A block diagram of this is shown in Fig. 9. The target mirror and lamp drive servos were simulated by ideal second-order transfer functions with 25 rad/sec natural frequency and damping ratio of 0.7 critical. The block labeled sky-Earth projector servos includes the representation of four rate-augmented position servos with a complete definition of the torque coupling between gimbal axes. The projection geometry that was included for later use in the synchronization studies compares the separate motions of two light vectors: one defined by the sky-Earth projector and the other by the target projector. This comparison was used to evaluate synchronization between the two scenes for simulated aircraft maneuvers.

The gimbal equations of motion were derived using the classical Euler method[4] of summing the moments applied to each gimbal. Each gimbal was assumed to be a rigid body and all gravitational torques and torques due to the rectilinear lamp drives were neglected. This resulted in 10 equations (three for each of the inner gimbals and one for the fourth gimbal since it has only one degree of freedom). Four of these equations were used to define the gimbal angular accelerations as:

$$I_{z\psi}\ddot{\psi} = T_\psi - I_{z\psi}\dot{R}_\theta \quad (5)$$

$$I_{y\theta}\ddot{\theta} = T_\theta - L_{\psi\theta}\sin\psi - M_{\psi\theta}\cos\psi - I_{y\theta}\dot{Q}_\phi - P_\theta R_\theta(I_{x\theta} - I_{z\theta}) \quad (6)$$

$$I_{x\phi}\ddot{\phi} = T_\phi - L_{\theta\phi}\cos\theta - N_{\theta\phi}\sin\theta - I_{x\phi}(\cos\beta)\ddot{\alpha} - Q_\phi R_\phi(I_{z\phi} - I_{y\phi}) \quad (7)$$

$$I_{x\alpha}\ddot{\alpha} = T_\alpha - (N_{\phi\alpha}\cos\phi + M_{\phi\alpha}\sin\phi)\sin\beta - T_\phi\cos\beta \quad (8)$$

Equation (5) is derived assuming that $I_{y\psi} = I_{z\psi}$. In Eqs. (5–8), the variables P_i, Q_i, and R_i and $\dot{P}_i$, $\dot{Q}_i$, and $\dot{R}_i$ define the instantaneous angular rates and accelerations, respectively, of each gimbal and may be expressed in terms of the gimbal angular accelerations, rates, and positions. The terms T_ψ, T_θ, T_ϕ, and T_α represent the gimbal drive torques and the terms $L_{\psi\theta}\sin\psi$, $M_{\psi\theta}\cos\psi$, $L_{\theta\phi}\cos\theta$, $N_{\theta\phi}\sin\theta$, $M_{\phi\alpha}\sin\phi$, and $N_{\phi\alpha}\cos\phi$ represent torques transmitted between the respective gimbals. These latter terms were defined by means of the six remaining Euler equations mentioned above. Equations (5–8) must be operated on algebraically to put them in an explicit form that is more suitable for computer solution.

Table 2 Aircraft body rates used in constant rate test cases, rad/sec

p	q	r
0	3	0
6	3	0
4	2	1
8	0	0

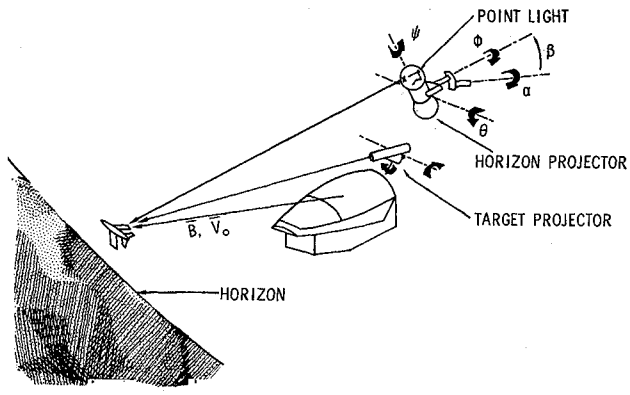

Fig. 10 Projection geometry.

To provide a means of checking the torque coupling math model, an independent derivation of Eqs. (5–8) was made using the Lagrange formulation. This method is a more direct mathematical approach, but the physical picture of the torques transmitted from gimbal to gimbal about each axis is not as obvious as in the Euler formulation.

Several dynamic check cases were run on the computer and compared with analytical solutions as a means of checking the computer solution. Each of these test cases was run assuming that T_ψ, T_θ, T_ϕ, and T_α in Eqs. (5–8) were zero. The complexity of a complete four-axis check made a general analytical solution unobtainable; therefore, it was necessary that these check cases exercise only portions of the system at one time. One of these check cases treated the inner three gimbals as a gyroscope mounted in a two-gimbal system. Using classical techniques, it is possible to predict the torque-free motion of the system for a given set of initial values of gimbal rates and positions. A second analytical solution of the complete four-axis system was obtained for a very restricted case of initial conditions using a variation of the Lagrange method developed by Routh.[5]

8.3 Projection Geometry

Figure 10 illustrates the projection geometry that was used to evaluate the synchronization of the target and horizon displays. As illustrated in the figure, the vectors $\bar{B}$ and $\bar{V}_0$ defined the angular positions (relative to the observer) of light rays in the target image and horizon scenes which are ideally coincident as shown in the figure. The angular differences between the X, Y, and Z components of $\bar{B}$ and $\bar{V}_0$ were recorded as ΔX, ΔY, ΔZ and used as the basis for synchronization evaluation.

The vector $\bar{B}$ was defined in terms of the target mirror gimbal center offset from the sphere center and the angular positions of the two projection mirrors. Similarly, vector $\bar{V}_0$ was defined in terms of sky-Earth gimbal offset, gimbal angular orientation, and the position of the point light source relative to the inner gimbal.

8.4 Test Cases

As a method of evaluating the over-all system performance, two sets of test cases were run using different combinations of simulated aircraft body rates. The first set of cases used constant values of p, q, and r modified by a first-order lag to control the onset acceleration. The particular rate values are shown in Table 2 and were chosen to create gimbal motions over a wide range of rates and acceleration where all rates are given in rad/sec.

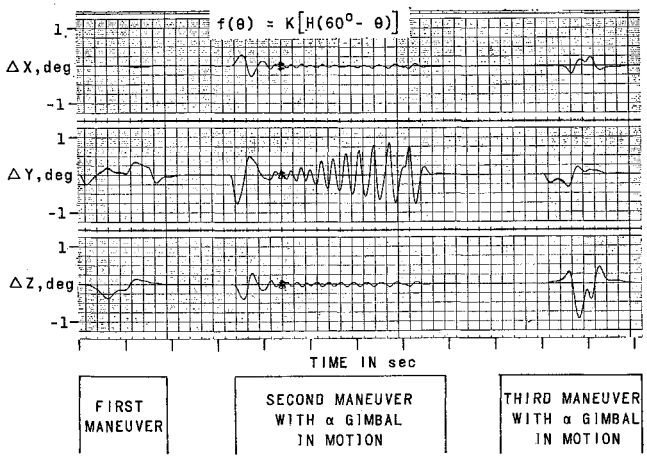

Fig. 11 Projection errors for simulated maneuvers with drive equation (3).

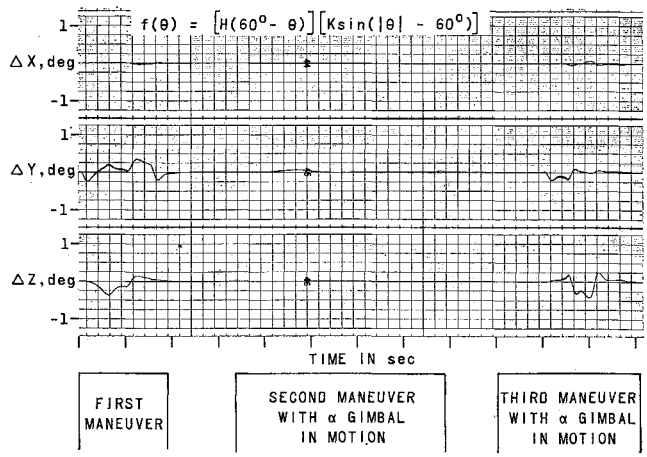

Fig. 12 Projection errors for simulated maneuvers with drive equation (4).

These spin vectors were used with a variety of possible initial values of α and aircraft pitch attitude and with an optimum value of K in drive equation (3). Equation (4), which is a refinement of Eq. (3), had not been developed at the time these cases were run. Analysis of these cases revealed that during the onset of α gimbal motion, the maximum values of the ψ gimbal rates and accelerations exceeded the original design specifications. As a result, the system design was modified to increase servo performance.

Although the constant rate cases outlined in Table 2 were used in initial hardware evaluation, it was recognized that these were far more extreme than normal flight maneuvers. Therefore, a second set of test cases were run using computer-generated profiles of the aircraft body rates as inputs to the gimbal simulation. These body rate profiles were based on typical aircraft maneuvers (e.g., split S, spiral, or loop) in which the normal acceleration did not exceed $4g$ at Mach 1. These profiles generated gimbal rates and accelerations of such a magnitude as to verify the sufficiency of the rate and torque limits of the system. To further study the design margins of individual servos, the same test cases were repeated at twice the amplitude of p, q, and r. Figure 11 illustrates a typical time history taken from one of these test cases with the separate phases of the maneuver labeled on the abscissa. The fourth gimbal drive equation used in this case was Eq. (3) and the variables recorded are the angular separations between target and horizon described in the section on projection geometry. One degree of angular separation corresponds to 4 in. of separation on the screen. Relatively large amplitudes of angular separation may be observed during the periods of fourth gimbal motion. The oscillatory nature of these separation errors is due to the transient behavior of the system as the fourth gimbal is repeatedly turned on and off by drive equation (3). Further study of the fourth gimbal drive led to the form of Eq. (4) for the fourth gimbal drive. The degree of improvement during fourth gimbal motion using Eq. (4) for the same maneuver is evident in Fig. 12. The remaining errors are due to torque coupling between gimbal axes and small variations in the response of individual servos due to inertia changes as the gimbals change relative orientation with respect to each other.

9. Concluding Remarks

This paper has presented a broad picture of the over-all design effort that has been devoted to the dual wide angle visual simulator. The performance characteristics of the various subsystems have been described. Finally, a more detailed picture has been given of the analysis carried out that has resulted in a suitable formulation of the sky-Earth projector fourth-axis gimbal drive. The resulting system, which is anticipated to be operational in early 1971, will add materially to the flight control research capabilities of the Langley Research Center.

References

[1] Mitchell, E. E. L. and Rogers, A. E., "Quaternion Parameters in the Simulation of a Spinning Rigid Body," *Simulation*, Vol. 4, No. 6, June 1965, pp. 390–396.

[2] Wilson, J. W., "Four Gimbal Systems for Simulation Display," *Simulation*, Vol. 12, No. 3, March 1969, pp. 115–120.

[3] Wilson, J. W., "Analysis and Mechanization of Three- and Four-Gimbal Systems," TN D-4689, Aug. 1968, NASA.

[4] Goldstein, H., "The Rigid Body Equations of Motion," *Classical Mechanics*, Addison Wesley, Reading, Mass., 1959, pp. 143–180.

[5] Wells, D. A., "Small Oscillations About Steady Motion," *Lagrangian Dynamics*, Schaum Publishing Co., New York, 1967, pp. 234–249.